The effects of a nonlinear delayed feedback on a chemical reaction

T. Chevalier, A. Freund, and J. Ross

Citation: The Journal of Chemical Physics **95**, 308 (1991); doi: 10.1063/1.461488
View online: http://dx.doi.org/10.1063/1.461488
View Table of Contents: http://scitation.aip.org/content/aip/journal/jcp/95/1?ver=pdfcov
Published by the AIP Publishing

The effects of a nonlinear delayed feedback on a chemical reaction

T. Chevalier,[a] A. Freund,[b] and J. Ross
Department of Chemistry, Stanford University, Stanford, California 94305

(Received 29 January 1991; accepted 4 March 1991)

With delay feedback experiments on the minimal bromate oscillator, we show that chemical systems with delay display a variety of dynamical behavior. Using a nonlinear delayed feedback, we induce Hopf bifurcations, period doubling, bifurcations into chaos, and crisis (observed for the first time in a homogeneous chemical system) into the system, which does not display this behavior without the delay. We test a conjecture [M. Le Berre, E. Ressayre, A. Tallet, H. M. Gibbs, D. L. Kaplan, and M. H. Rose, Phys. Rev. A **35**, 4020 (1987)] that the dimension of a chaotic attractor is equal to τ/δ_f, where τ is the delay time and δ_f is the correlation time of the delayed feedback. Using the Grassberger–Procaccia algorithm [P. Grassberger and I. Procaccia, Physica **9D**, 189 (1983)] to calculate the dimensions of the chaotic attractors from the experimental system, we show that the calculated dimensions are less than those calculated by τ/δ_f. We compare numerical integrations of the proposed mechanism for the minimal bromate oscillator with the experimental results and find agreement of the predicted bifurcation sequence with the experimental observations. The results of this study indicate that with appropriate delay feedback functions, and a sufficiently nonlinear dynamical system, it is possible to "push" a dynamical system into further bifurcation regimes, of interest in themselves, which also yield information on the system without delay.

I. INTRODUCTION

Many kinetic processes can be described by differential delay equations of the form

$$dx(t)/dt = f[x(t), x(t-\tau)]. \quad (1)$$

Functional delay differential equations with retarded arguments, such as Eq. (1), have been used to model diverse phenomena such as the regulation of enzyme synthesis,[1] the control of hematopoiesis[2,3] the problem of balancing a stick upon one's fingertips,[4] instabilities in optically bistable systems,[5] and the dynamical behavior of certain gas evolution oscillators.[6] Schell and Ross[7] studied the response of photoilluminated thermochemical reactions to a delayed feedback. Epstein[8] has investigated the effects of delay on some simple linear models for an electrochemical cell, the process of nucleation in a solid-state reaction, and a model of diffusion through a membrane.

The introduction of a delay in a dynamical system often leads to a change in the stability properties of the system. Zimmermann, Schell, and Ross[9] introduced a delayed feedback in order to stabilize the unstable branch of the bistable $S_2O_6F_2/SO_3F$ illuminated thermochemical system. They also observed that short delay times lead to the creation of limit cycles via a subcritical Hopf bifurcation. In another experiment involving a chemical system with delay, Weiner, Schneider, and Bar-Eli[10] examined the effects of a delayed feedback on a chemical oscillator, the minimal bromate oscillator (MBO) system. They observed that the period of the autonomous oscillations in the system increased and decreased in a "sawtooth" fashion as a function of the delay.

In our studies on the effects of nonlinear delayed feedback on chemical systems, we are interested in two goals—(a) the introduction of dynamical complexity into a chemical system and (b) the use of a delay feedback as a means by which to probe a chemical mechanism.

Since differential delay equations, which are infinite-dimensional systems, can display great dynamical complexity in their behavior,[11] we use a delayed feedback in a chemical system, which by introducing additional dynamical complexity into the system, gives information on the dynamics of the system without delay. The imposition of delays on a chemical reaction does not alter the mechanism of the reaction. In a subsequent paper, we will show how one can use a delayed feedback to gain information about the mechanism of a chemical reaction, i.e., how a delayed feedback can be used to (a) determine the elements of the steady state Jacobian and thus (b) differentiate among competing mechanisms.

We focus our work on one particular chemical system—the minimal bromate oscillator. The MBO system displays bistability[12] and possesses a narrow oscillator[13] regime when run in a CSTR (continuous-flow, stirred-tank reactor). With the flows and concentrations used in our studies, the MBO system, without delay, only displays multiple stationary states; it does not oscillate.

In our studies on the MBO system, we use the concentration of Br^- in the chemical reactor at an earlier time $t-\tau$ to control the flow of Br^- into the reactor at time t. With the nonlinear delayed feedback, the MBO system displays complex behavior. In Sec. II, we describe both the experimental apparatus used in the MBO studies and the method used to implement the delayed feedback. In Sec. III, we discuss the wide range of dynamical behavior observed when the MBO system is subjected to a delayed feedback—period doubling, chaos, and multiple attractors. The birth of a limit cycle, arising from the delayed feedback, is clearly exhibited in Sec. III B. Upon a continuous change in the delay time, we can induce the system to undergo the familiar period doubling route to chaos (Sec. III C). Using the Grassberger–

[a] Present address: Stanford Synchrotron Radiation Laboratory, Stanford, CA 93305.
[b] Present address: Institute of Physik Chemie, 8700 Wurburg, Germany.

 0021-9606/91/130308-09$03.00

Procaccia[14] algorithm, we calculate the correlation dimension for a number of chaotic attractors of the MBO system in Sec. III E. For dynamical systems with a delayed feedback, it has been conjectured[15,16] that the dimension of a chaotic attractor is approximately equal to τ/δ_f, where δ_f is the correlation time of the delayed feedback. Using the calculated correlation dimensions, we test this conjecture in Sec. III D and find that for our system, τ/δ_f overestimates the correlation dimension. In Sec. III E, we show how the use of the delayed feedback allows us to create coexisting attractors; in addition, we show a sequence in which one of the attractors experiences a sudden jump in size upon a change in the delay time. This is, to our knowledge, the first experimental evidence of crisis in a homogeneous chemical system. In Secs. IV and V, we discuss a simulation of the minimal bromate oscillator system with a delayed feedback. We show that bifurcation features seen in the experimental system are also present in the simulated system.

II. EXPERIMENTAL METHODS AND PROCEDURES

The reaction is conducted in a 27.0 ml CSTR fed by three inlet lines. Two fixed speed 20 rpm peristaltic pumps operating at a flow rate of 1.85 ml min^{-1} are used for introducing the $MnSO_4$ (8.0×10^{-4} M in 0.25 M H_2SO_4) and $NaBrO_3$ (0.25 M in 0.25 M H_2SO_4) solutions into the CSTR. A magnetically coupled gear pump operating at 0–6 ml min^{-1} is used to pump in the sulfuric acid solution of NaBr (8.0×10^{-4} M in 0.25 M H_2SO_4). The CSTR and all feed solutions are thermostated to 25.5 °C; the stirring rate in the CSTR is maintained at 750 rpm. See Fig. 1 for the experimental setup.

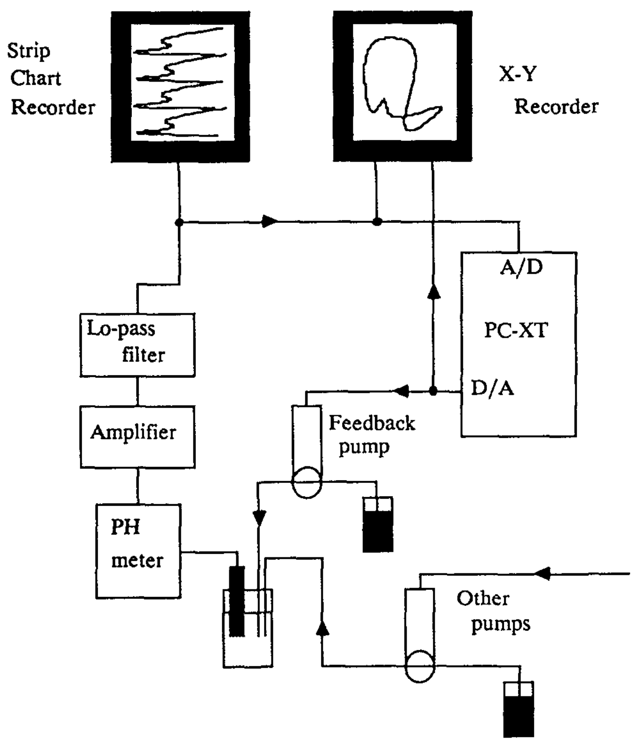

FIG. 1. A schematic diagram of the experimental setup. The CSTR is fed by three gear pumps. (Br^-), The bromide concentration, measured by the ion-selective electrode at time t, is used to control the (Br^-) inlet pump at time $t+\tau$.

The dynamics of the reaction is monitored with a bromide ion-selective electrode (Orion Research). The signal from the electrode is digitized by a 12-bit A/D converter (Data Translations) before being recorded and stored by an IBM PC-XT computer. The flow rate for the NaBr pump is varied every 0.22 s (the sampling time) according to Eq. (2),

$$f_{Br^-}(t) = \kappa[1+\epsilon\sin(\omega x_\tau+\phi)], \quad (2)$$

where $x_\tau \equiv x(t-\tau)$ represents the voltage reading [proportional to $-\log(Br^-)$] obtained τ time units earlier from the ion-selective electrode, κ is the baseline level for the flow, ϵ controls the amplitude of the nonlinear feedback, ω represents a frequency in concentration space, and ϕ is the phase of the feedback.

III. MEASUREMENTS AND RESULTS

A. Behavior in the absence of delay

With the flow rates and concentrations used and in the absence of delay, the MBO system displays hysteresis when the Br^- flow is used as an adjustable constraint (Fig. 2). As shown in Fig.3, the steady states of the MBO system with delay are found at the intersection(s) of the hysteresis curve from Fig. 2 and the curve defined by Eq. (1). The introduction of a delay does not alter the possible steady states of the system; it may alter the stability properties of the steady states.[17]

B. Birth of a limit cycle—supercritical Hopf bifurcation

Figures 4 and 5 show the results of an experiment to determine the onset and growth of a limit cycle in the MBO

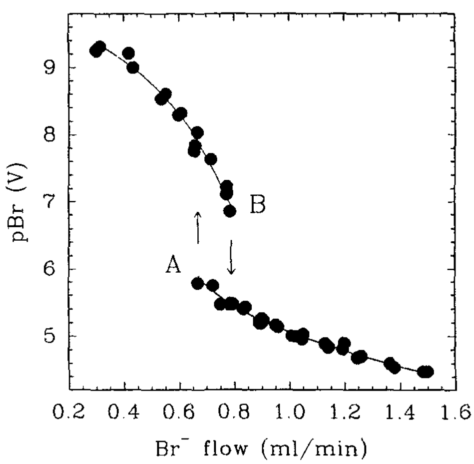

FIG. 2. The experimentally determined hysteresis for the MBO system, without delay, plotted in the (pBr_{ss}, f_{Br^-}) plane. Fixed constraints: $f_{Mn^{2+}}$ = 1.85 ml min^{-1}, $f_{BrO_3^-}$ = 1.85 ml min^{-1}, $(Mn^{2+})_0 = 8.0\times10^{-4}$ M, $(BrO_3^-)_0 = 0.25$ M, $(Br^-)_0 = 8.0\times10^{-4}$ M, $(H^+)_0 = 0.25$ M, and T = 25.5 °C. The reactor volume is 27.0 ml. Experimental points are from two separate experiments conducted over a month apart. Point A (B) marks the left (right) marginal stability point. The hysteresis curve represents the underlying dynamical behavior of the MBO system for the experimental constraints listed.

system with a delayed feedback. In these experiments, $\kappa = 1.465$ ml min^{-1}, $\epsilon = 1.0$, $\omega = 2.574$ V^{-1}, and $\phi = 0.0$ [Eq. (2)]; the delay time τ is used as the bifurcation parameter. For values of the delay less than a critical time $\tau_c \approx 6.6$ s, the system relaxes to a single stationary state. For values of τ greater than τ_c, the originally stable steady state becomes unstable and the system is attracted to a limit cycle. As the delay time is increased further, the amplitude of the oscillations grows.

Figure 4 is a plot of the amplitude as a function of $\tau - \tau_c$ which is well fitted with the equation

$$A \sim (\tau - \tau_c)^{\alpha}. \tag{3}$$

From the data presented in the figure, α is found to be $\alpha = 0.47 \pm 0.03$ with $\tau_c = 6.6 \pm 0.3$ s. This value for α is in good agreement with the value ($\alpha = 0.5$) predicted for a generic supercritical Hopf bifurcation.[18] Figure 5 shows that the period of the oscillations varies linearly with the distance from the bifurcation value ($\tau - \tau_c$), which also agrees with the variation predicted for a supercritical Hopf bifurcation.

C. Period doubling

Among the bifurcations that a limit cycle can undergo is one of period doubling. Period doubling sequences have been observed in Rayleigh–Bénard convection experiments,[19] the Belousouv–Zhabotinskii reaction,[20] in the response of the pupil light reflex to a delayed feedback,[21] and other experimental systems. In Figs. 6–8, we present the first experimental evidence for period doubling in a chemical system with a delayed feedback.

Figure 6 shows reconstructed phase portraits[22,23] in the [pBr(t), pBr($t + \delta$)] plane with a lag δ equal to 32.96 s. In this sequence of experiments, $\kappa = 1.465$ ml min^{-1}, $\epsilon = 1.0$, $\omega = 2.574$ V^{-1}, and $\phi = 0.0$. In the experimental series, the original limit cycle [Fig. 6(a)] with a τ value of 8.24 s and a period T of 35.52 s undergoes a period doubling bifurcation

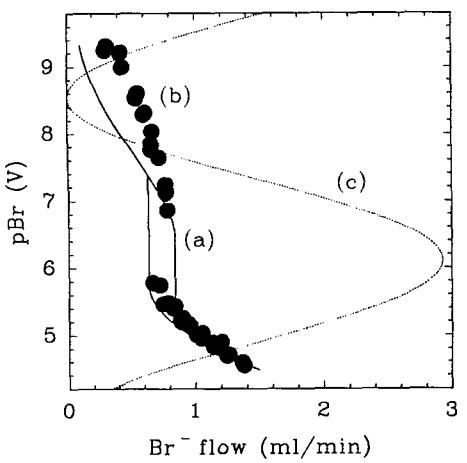

FIG. 3. A combined plot of both the (a) calculated (Sec. IV) and (b) experimental hysteresis and (c) a feedback curve [Eq. (1)] with parameters $\kappa = 1.465$ ml min^{-1}, $\epsilon = 1.0$, $\omega = 1.287$ V^{-1}, and $\phi = 0.0$. The intersections of the feedback curve with the hysteresis curve determine the locations of the steady states.

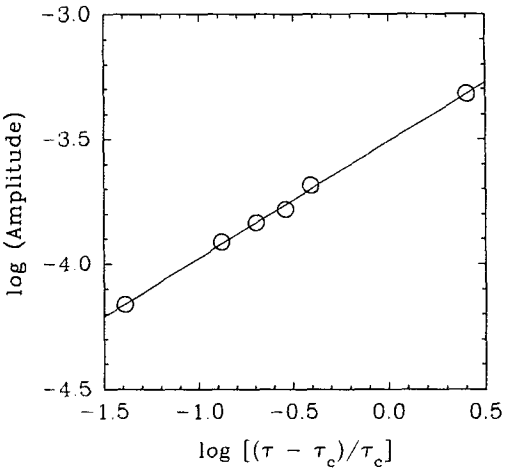

FIG. 4. The amplitude of the periodic oscillation vs $(\tau - \tau_c)/\tau_c$ plotted on a log–log scale. The solid line is a least-squares fit to Eq. (3), yielding $\alpha = 0.47$.

[Fig. 6(b)] when τ is increased to 32.96 s. As τ is increased further, we observe a $4T$ orbit ($T = 202.8$ s, $\tau = 43.94$ s) [Fig. 6(c)], an $8T$ orbit ($T = 317.2$ s, $\tau = 54.92$ s) [Fig. 6(d)], and, finally, a chaotic trajectory at a value of $\tau = 219.70$ s [Fig. 6(e)].

In order to demonstrate that other parameters besides the delay time τ can be used as bifurcation parameters, we adjusted the phase ϕ of the feedback in a series of experiments. A change in ϕ results in a change in the location of the steady state. In these experiments, the delay is kept constant ($\tau = 109.85$ s). With $\kappa = 2.5$ ml min^{-1}, $\epsilon = 0.8$, $\omega = 1.257$ V^{-1}, and $\phi = 15.712$, the system is attracted to a fixed point [Fig. 7(a)]. As ϕ is decreased to 14.141, the fixed point is no longer stable—the trajectory is attracted to a stable limit cycle [Fig. 7(b)]. With further decreases in ϕ, the system shows a period doubled orbit {$\phi = 13.355$ [Fig. 7(c)]} and a chaotic trajectory {$\phi = 12.570$ [Fig. 7(d)]}.

D. Chaotic trajectories and dimension calculations

The generalized dimensions of an attractor, which measure its static properties, have become the most commonly

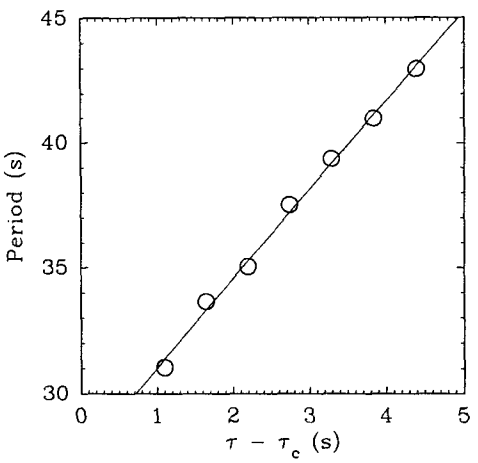

FIG. 5. The period of supercritical Hopf bifurcation as a function of $\tau - \tau_c$.

used criteria for characterizing chaotic dynamical systems.[24]

Generalized dimensions are defined as follows: given a strange attractor in an m-dimensional space and a finite section of a discretized trajectory $\mathbf{X}_i$, $i = 1,2,...,N$ on the attractor, cover the phase space with a mesh of boxes of size r^m. If $M(r)$ is the total number of boxes containing the points of $\mathbf{X}_i$, then the probability p_k of finding a point of the trajectory in box k is given by

$$p_k = \lim_{N\to\infty} \frac{N_k}{N}, \tag{4}$$

where N_k is the number of points from the trajectory in box k.

The static structure of the attractor is defined[25,26] through the qth power of p_k:

$$D_q = \frac{1}{q-1} \lim_{r\to 0} \frac{\log(\Sigma_{k=1}^{M(r)} p_k^q)}{\log r}, q \geqslant 0. \tag{5}$$

Generalized dimensions with integral q correspond to the exponents associated with q-ordered correlation func-

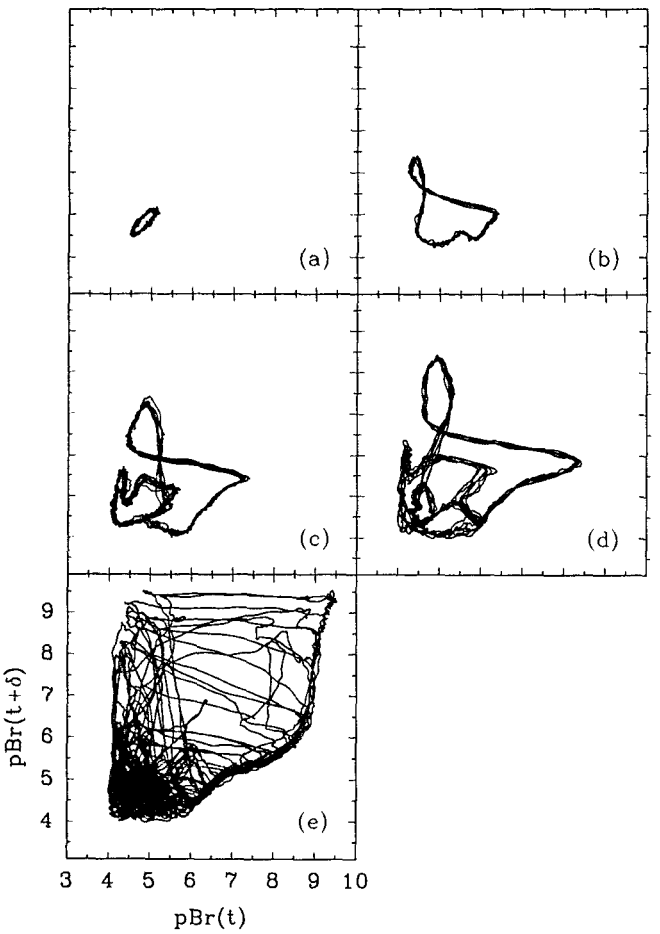

FIG. 6. Period doubling bifurcation as τ is varied. Phase portraits for five values of τ in the [pBr(t), pBr($t+\delta$)] plane, where pBr ($t+\delta$) is proportional to the log of the Br^- potential at time $t(t+32.96$ s). The feedback function parameter values are $\kappa = 1.465$ ml min^{-1}, $\epsilon = 1.0$, $\omega = 2.574$ V^{-1}, and $\phi = 0.0$. The nT period and τ values are: (a) $1T$, $\tau = 8.24$ s; (b) $2T$, $\tau = 32.96$ s; (c) $4T$, $\tau = 43.94$ s; (d) $8T$, $\tau = 54.92$ s; and (e) chaotic, $\tau = 219.70$ s.

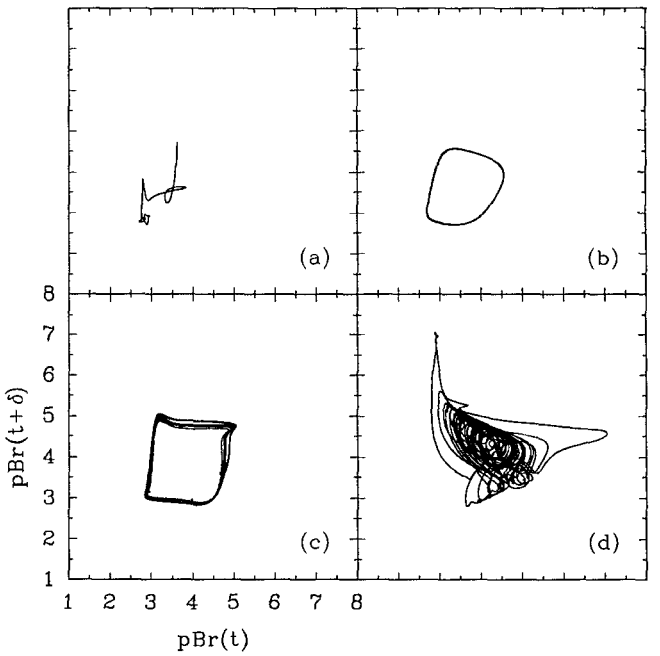

FIG. 7. An example of a period doubling bifurcation as ϕ is varied. Phase portraits for four values of ϕ in the [pBr(t), pBr($t+\delta$)] plane $\delta = 54.92$ s). The feedback function parameter values are $\kappa = 2.5$ ml min^{-1}, $\epsilon = 0.8$, $\omega = 1.257$ V^{-1}, and $\tau = 109.85$ s. The nT period and ϕ values are (a) stable focus, $\phi = 15.712$; (b) $1T$, $\phi = 14.141$; (c) $2T$, $\phi = 13.355$; and (d) chaotic, $\phi = 12.57$.

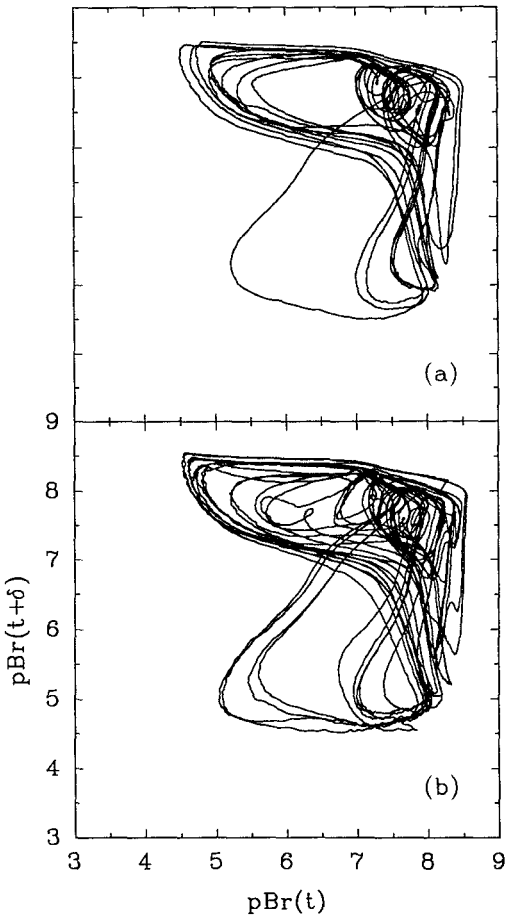

FIG. 8. Phase portraits for two of the experimental chaotic trajectories used in the dimension calculations. The feedback function parameter values are $\kappa = 1.0$ ml min^{-1}, $\epsilon = 1.0$, $\omega = 1.047$ V^{-1}, and $\phi = 10.47$. The delay values are: (a) $\tau = 131.82$ s and (b) $\tau = 175.76$ s.

tions. Hentschel and Procaccia[25] have shown that the D_q are ordered such that $D_q \geqslant D_{q'}$ for any $q' \geqslant q$. Of the infinite number of generalized dimensions, three have been studied extensively—the Hausdorff dimension D_0, the information dimension D_1, and the correlation dimension D_2.

The correlation dimension, defined as

$$D_2 = \lim_{r \to 0} \frac{\log(\Sigma_{k=1}^{M(r)} p_k^2)}{\log r}, \tag{6}$$

is the most widely used of the measures of chaotic behavior.[27]

Since it is not often possible to determine experimentally an m-dimensional trajectory by the simultaneous measurement of m independent signals, some method is needed for describing an experimental time series in an m-dimensional phase space. The standard method for reconstructing a phase space trajectory from time series data is the "method of delays."[22,23] Given a time series, with sampling intervals Δt_s, the discretized experimental trajectory is described by a vector

$$v(k) \equiv v(k\Delta t_s) | k = 1,2,...,N_T. \tag{7}$$

The time series is embedded in an m-dimensional phase space by means of the vectors

$$\begin{aligned} y(1) &= \{v(1),v(1+L),...,v[1+(m-1)L]\}, \\ y(2) &= \{v(1+J),v(1+J+L),...,v[1+J+(m-1)L]\}, \\ &\vdots \\ y(p) &= \{v[1+(p-1)J],v[1+(p-1)J+L],..., \\ &\quad v[1+(p-1)J+(m-1)L]\}, \ \ldots . \end{aligned} \tag{8}$$

In Eq. (8), L is the number of sampling intervals Δt_s between successive components of an embedding vector, J is the number of sampling intervals between first components of successive vectors, and $(m-1)L$ is the window length of the embedding.

Grassberger and Proccacia[14] showed that the "correlation integral"

$$C_m(N,r) = \frac{2}{N(N-1)} \sum_{1 \leqslant i,j}^{N} \Theta(r - \|x_i - x_j\|), \tag{9}$$

where $\Theta(x)$ is the Heaviside step function, is related to the correlation dimension D_2 by

$$D_2 = \lim_{m \to \infty} \lim_{r \to 0} D_2(m;r). \tag{10}$$

In Eq. (10),

$$D_2(m;r) = \frac{d[\ln C_m(N,r)]}{d[\ln(r)]} \tag{11}$$

is the slope of the log–log plot of $C_m(N,r)$ vs r. One generally calculates the correlation dimension by calculating the correlation integral for a series of embedding dimensions. One then looks for a plateau in the plots of $d[\ln C_m(N,r)/d[\ln(r)]]$ vs $\ln(r)$. If the plateau is common to a number of embedding dimensions, the value of the slope at the plateau is used as the correlation dimension.

In applying Eq. (9) to measurements, it is readily apparent that (1) neither of the limits in Eq. (10) can be achieved and (2) the range of r and m over which the correlation integral is calculated is limited by noise (restricts the smallest r used) and data set size (restricts the largest m used). In order to avoid artificial correlations for small data sets, it has been suggested[28] that the Grassberger–Procaccia algorithm be modified so that one uses

$$C_m(r,N,W) = \frac{2}{N(N-1)} \sum_{i=W}^{N} \sum_{j=1}^{N-i} \Theta(r - \|x_i - x_j\|) \tag{12}$$

in place of Eq. (9). The use of W in Eq. (12) allows one to avoid artificial correlates in the summation; instead, only vectors which are not too closely spaced in time are used in the summation. [Note that for $W = 1$, Eq. (12) reduces to Eq. (9).]

Three numerical studies on dynamical systems driven by a delayed nonlinear feedback have found that the Lyapunov dimension d_L increases linearly with the delay time τ. Farmer,[29] in his study of the equations derived by Mackey and Glass[3] for modeling white blood cell production, was the first to observe the linear increase in d_L with the delay. The other two examples are from the study of a delayed feedback in optical systems—the plane-wave ring cavity[30] and an electro-optic hybrid system.[16]

The Lyapunov dimension, an upper bound to the information dimension, is defined[31] by

$$d_L = j + \frac{\Sigma_{i=1}^{j} \lambda_j}{\|\lambda_j + 1\|}, \tag{13}$$

where j is the largest integer for which $\Sigma_{i=1}^{j} \lambda_j > 0$. (By convention, the Lyapunov exponents λ_i are ordered such that $\lambda_1 \geqslant \lambda_2 \geqslant \cdots \geqslant \lambda_d$). It has been conjectured[31] that d_L is approximately equal to the Hausdorff dimension D_0.

For dynamical systems with a delayed feedback, it has been further conjectured[15,16] that the Lyapunov dimension of the chaotic attractor is equal to τ/δ_f, where δ_f is the correlation time of the delayed feedback. Le Berre *et al.*[15] point out that the interaction between the dynamical system and the delayed feedback can be seen as a set of "kicks" of mean duration δ_f. During each delay period τ, the system undergoes τ/δ_f kicks. Each of these kicks are loosely independent in that the nth kick during the k th delay period is only correlated with the nth kick during the $(k+1)$-st delay period. From this follows their conjecture that the number of independent kicks should be the effective number of degrees of freedom in the system.

Since the Hausdorff dimension D_2 serves as an upper bound on the correlation dimension D_0, it is possible to test the conjecture of Le Berre *et al.* by calculating the correlation dimension of attractors in the MBO system with a delayed feedback.

We used the Grassberger–Procaccia algorithm with Theiler's suggested modification [Eq. (12)] to calculate the correlation dimension for some of the complex attractors of the MBO system (see Fig. 8 for the phase portraits). Figure 9 shows the results of the calculations on the experiments of Fig. 8. In each of the calculations, the attractor is embedded into four, six, eight, ten, or 14 dimensions. The lag L for the reconstruction is determined such that the window length

$(m-1)L$ is two to three times the correlation time δ_f. The correlation time δ_f, in turn, is defined as the time required for the autocorrelation function to decay to e^{-1} of its original value.[32] The correlation dimension is determined by finding the plateau in the plot of $d[\ln C(r,N,W)]/d[\ln(r)]$ (see Fig. 9).

As a test of Le Berre's *et al.* conjecture that the dimension of chaotic attractors for dynamical systems driven by a delayed nonlinear feedback is equal to the delay divided by the correlation time of the delayed feedback, we calculate the correlation times δ_f for the feedbacks used in the experiments. Figure 10 is a plot of the relationship between τ/δ_f, the correlation dimension D_2, and τ. As can be seen in the figure, both methods show that the correlation dimension does increase as the delay time increases. As predicted, the dimension, as calculated by τ/δ_f, is higher than the dimension that calculated by the Grassberger–Proccacia algorithm.

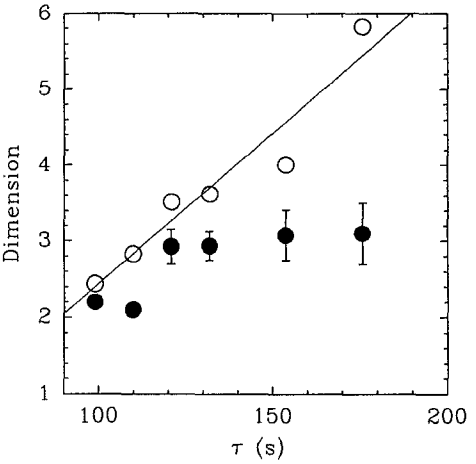

FIG. 10. The calculated correlation dimension and τ/δ_f as a function of τ. The open circles correspond to the correlation to the dimension as calculated by τ/δ_f; the filled circles are determined from the Grassberger–Proccacia algorithm.

E. Coexisting attractors and crisis

Among the varied dynamical behavior of chemical systems maintained far from equilibrium is multistability, for a given set of constraints, one or more attractors may exist simultaneously. Depending on the initial conditions, the asymptotic behavior of the system may be a simple stationary state, a limit cycle, a quasiperiodic trajectory, or a chaotic trajectory.

We have observed a variety of types of multistability in the MBO system with a delayed feedback—a stationary state coexisting with another stationary state, a stationary state with a limit cycle, a stationary state with a chaotic attractor, a limit cycle with another limit cycle (birythmic), and a limit cycle with a chaotic attractor.

In Fig. 11, we present one example of coexisting limit cycles where each limit cycle is associated with a separate fixed point. For the feedback values used ($\kappa = 1.465$ ml min^{-1}, $\epsilon = 1.0$, $\omega = 1.716$ V^{-1}, and $\phi = 0.0$), the system possesses three fixed points. Initially, i.e., at $\tau = 0$, two of the fixed points are asymptotically stable (the filled circles in Fig. 11); the third fixed point is unstable (the square in the figure). The insets of the unstable fixed point (a saddle) serve to separate the basins of attraction of the two stable fixed points. By adjusting the initial conditions of the experimental runs, specifically the Br^- flow for $0 \leqslant t < \tau$, we can choose the fixed point to which the system is attracted. As the delay is increased, each of the stable fixed points becomes unstable as each goes through a Hopf bifurcation.

With the initial $(0 \leqslant t < \tau)$ Br^- flow set to 2.5 ml min^{-1} and a τ value of 54.92 s, we find that the system relaxes to a $1T$-periodic limit cycle centered around the fixed point at high pBr potential. After flushing out the reactor contents and changing the initial Br^- flow rate to 1.83 ml min^{-1}, the system is attracted to a $4T$-periodic limit cycle which surrounds the fixed point at low pBr potential. (The original $1T$-periodic limit cycle has apparently undergone two period doubling.) Thus, for the parameter values used ($\kappa = 1.465$ ml min^{-1}, $\epsilon = 1.0$, $\omega = 1.287$ V^{-1}, $\phi = 0.0$, and $\tau = 54.92$ s, the MBO system exhibits birhythmicity. See Fig. 11(a) for the phase portrait at a τ value of 54.92 s.

With a different value for the delay ($\tau = 109.85$ s), the lower fixed point and the unstable fixed point (square) are both surrounded by a trajectory [Fig. 11(b)], regardless of

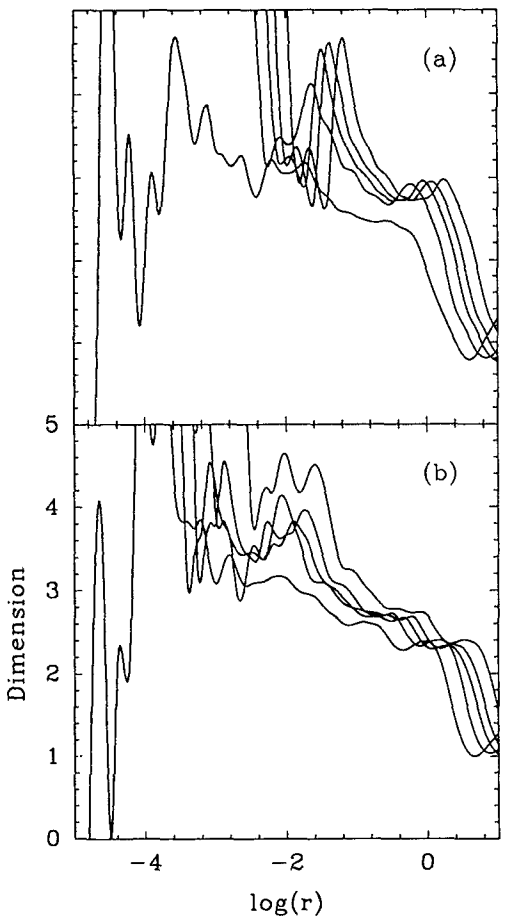

FIG. 9. The plot of $d[\ln C_m(r,N,W)]/d[\ln(r)]$ vs $\ln(r)$ for embedding dimensions 4,6,8,10, and 14. See Fig. 8 for values of the feedback parameters and τ.

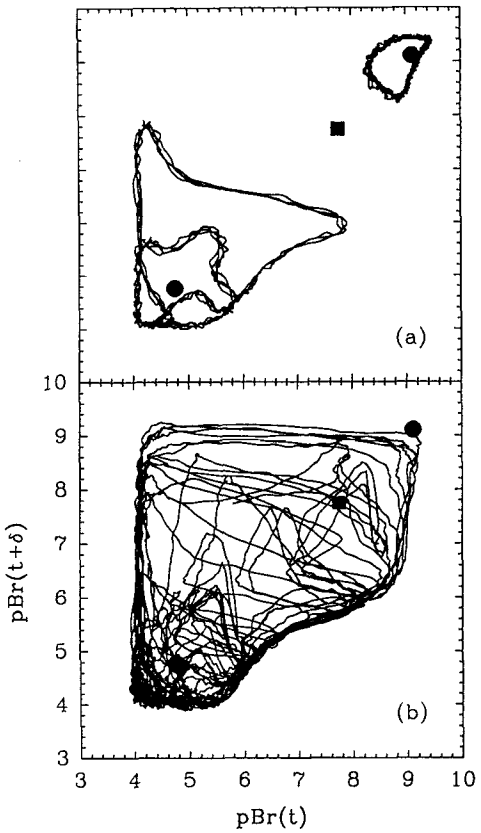

FIG. 11. An experimental example of multiple attractors. Phase portraits in the $[\mathrm{pBr}(t), \mathrm{pBr}(t+\delta)]$ plane with $\delta = 32.9$ s. The values for the feedback parameters are $\kappa = 1.465$ ml min^{-1}, $\epsilon = 1.0$, $\omega = 1.287$ V^{-1}, and $\phi = 0.0$. The delay τ is equal to: (a) 54.925 or (b) 109.85 s. The initial conditions for both (a) and (b) are upper pBr state attractor—$\mathrm{flow}_{\mathrm{Br}}$ $(t) = 2.5$ ml min^{-1}, lower pBr state attractor—$\mathrm{flow}_{\mathrm{Br}}$ $(t) = 1.83$ ml min^{-1} for $0 < t < \tau$. In both (a) and (b), the filled circles (filled square) represent initially stable (unstable) fixed points. Upon an increase in τ, the lower attractor undergoes a crisis of chaos upon colliding with the unstable fixed point.

the initial Br^- flow rate. We were not able to find a set of initial conditions that would lead to an attractor centered about the upper fixed point. We assume that a separate attractor for the high pBr potential state no longer exists. Because of the jump in the size of the low pBr potential attractor, we conclude that the lower pBr potential attractor has undergone a crisis of chaos[33] upon colliding with either the saddle point itself, or the saddle's inset. This, to our knowledge, is the first experimentally observed instance of crisis in a homogeneous chemical system.

IV. COMPUTATIONAL METHODS AND PROCEDURES

We compare some of the experiments on the minimal bromate reaction with numerical integration of a proposed mechanism for this reaction. The seven step minimal bromate oscillator mechanism, originally devised by Noyes, Field, and Thompson,[34] is shown below. The rate constants are given in Table I:

$$BrO_3^- + Br^- + 2H^+ \rightleftharpoons HBrO_2 + HOBr, \quad (R1)$$

$$HBrO_2 + Br^- + H^+ \rightleftharpoons 2HOBr, \quad (R2)$$

$$HOBr + Br^- + H^+ \rightleftharpoons Br_2 + H_2O, \quad (R3)$$

$$BrO_3^- + HBrO_2 + H^+ \rightleftharpoons 2BrO_2^{\cdot} + H_2O, \quad (R4)$$

$$Mn^{2+} + BrO_2^{\cdot} + H^+ \rightleftharpoons Mn^{3+} + HBrO_2 \quad (R5)$$

$$Mn^{3+} + BrO_2^{\cdot} + H_2O \rightleftharpoons Mn^{2+} + BrO_3^- + 2H^+, \quad (R6)$$

$$2HBrO_2 \rightleftharpoons BrO_3^- + HOBr + H^+. \quad (R7)$$

The differential equations, derived from the rate equations and flow terms, are of the form

$$\frac{dx_i}{dt} = R(x) + k_0(x_{i,0} - x_i). \quad (14)$$

In Eq. (14), $R(x)$ represents the kinetic terms derived from reactions (R1)–(R7), while $k_0(x_{i,0} - x_i)$ is the flow term associated with species x_i.

In order to match the experimental steady states of the reaction without a delayed feedback, we found that it was necessary to (1) change the inlet concentrations from the values used in the experiments and (2) use the so-called "Hi"[35] values for the kinetic rate constants. Using $[Br^-]_0 = 6.0\times10^{-4}$ M (vs 8.0×10^{-4} M), $[BrO_3^-]_0 = 0.40$ M (vs 0.25 M), $[Mn^{2+}]_0 = 7.0\times10^{-4}$ M (vs 8.0×10^{-4} M), and $[H^+]_0 = 0.275$ M (vs 0.25 M), the calculated hysteresis curve for the system without delay closely matches the experimental points (see Fig. 3).

In simulating the MBO reaction with a delayed feedback, we change the bromide flow f_{Br^-} at time t according to Eq. (2). Since the pumps used in the experiments are limited to a 0–6 ml min^{-1} range, the simulated bromide flow is constrained to lie within the same values. In Eq. (15), the bromide potential x is assumed to be a linear function of the log of the bromide concentration

$$x(t) = -1.8676 \log[Br^-(t)] - 5.474. \quad (15)$$

The slope and intercept used in Eq. (15) are derived from the characteristics of the amplified potential of the solid state bromide electrode used in the experiments.

The inverse residence time k_0 is related to the total flow f_0:

$$k_0(t) = V^{-1} f_0(t) = V^{-1}[f_{\mathrm{Br}^-}(t) + f_{BrO_3^-} + f_{Mn^{2+}}], \quad (16)$$

where $f_{BrO_3^-}$ and $f_{Mn^{2+}}$ are each held fixed at 1.85 ml min^{-1} and the volume V is 27.0 ml.

In order to maintain a close correspondence between the experimental system and the simulation, the basic time step

TABLE I. The "Hi" rate constants for the minimal bromate oscillator (MBO).

Reaction	k_f	k_r
(R1)	2.1 M^{-3} s^{-1}	1×10^4 M^{-1} s^{-1}
(R2)	2×10^9 M^{-2} s^{-1}	5×10^{-5} M^{-1} s^{-1}
(R3)	8×10^9 M^{-2} s^{-1}	110 s^{-1}
(R4)	7×10^3 M^{-2} s^{-1}	2×10^7 M^{-1} s^{-1}
(R5)	6×10^5 M^{-2} s^{-1}	5×10^7 M^{-1} s^{-1}
(R6)	9.6 M^{-1} s^{-1}	4.2×10^{-5} M^{-3} s^{-1}
(R7)	2×10^9 M^{-1} s^{-1}	1×10^{-8} M^{-2} s^{-1}

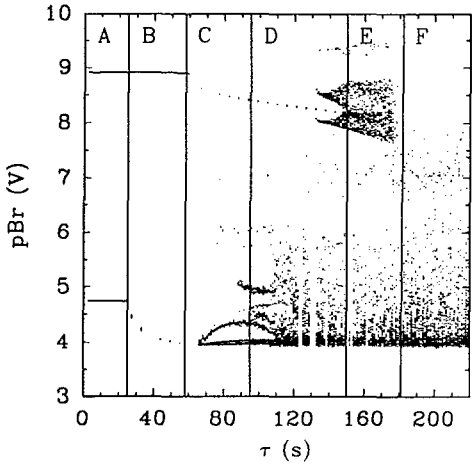

FIG. 12. A bifurcation diagram from numerical integration of the kinetic equations for the reaction mechanism (R1)–(R7). Solid lines represent stationary states, dots represent periodic or chaotic states. Region A contains two coexisting stationary states; B a stationary state and a limit cycle; C two coexisting limit cycles; and D a limit cycle and a chaotic attractor and E two coexisting chaotic attractors. Region F, with one attractor, occurs after the crisis. The feedback function parameter values are $\kappa = 1.465$ ml min^{-1}, $\epsilon = 1.0$, $\omega = 1.287$ V^{-1}, and $\phi = 0.0$.

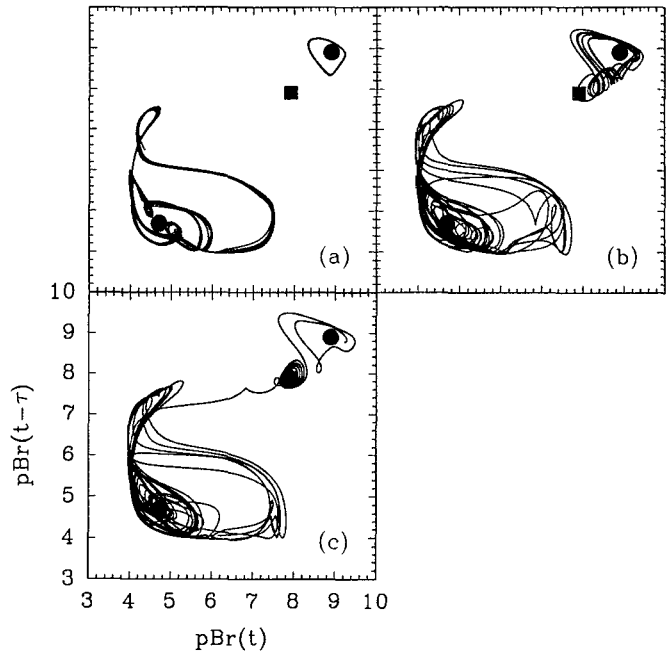

FIG. 13. Selected phase portraits from the bifurcation diagram. (a) A limit cycle and a *Pn* attractor. (b) Two chaotic attractors (shortly before the crisis point). (c) The phase portrait trajectory for the attractor in the high pBr range (shortly after the crisis). In the figure, the filled circles (filled square) represent initially stable (unstable) fixed points.

for the integration is set equal to the sampling time used in the experiments 0.22 s. Since the integration involves a delay term, a history of (Br^-) values must be maintained.

With the use of a modified Gear method, the integrations are continued until the system either reaches a steady state, or the final integration time is greater than or equal to 25 000 s. We specify the values of pBr($-\tau$) and pBr(0) and linearly interpolate for $-\tau < t \leqslant 0$ to set the initial conditions.

In the next section, we discuss the calculated behavior of the system without delay and some of the results obtained from a bifurcation diagram (Fig. 12) of the MBO system with delay. (For earlier usage of such plots, see Refs. 36 and 37.) For the bifurcation plot,[36] we have used a Poincaré map with a nonlinear cross section defined by $d\text{pBr}/dt = 0$. For each delay value ($0 \leqslant \tau \leqslant 220$ s) after the initial transient integration time, each occurrence of a local maximum in the pBr value is plotted. In the calculations for the bifurcation diagram, we use the same feedback parameters as those used in the experimental study of coexisting attractors and crisis (Sec. III E), i.e., $\kappa = 1.465$ ml min^{-1}, $\epsilon = 1.0$, $\omega = 1.287$ V^{-1}, and $\phi = 0.0$.

V. COMPUTATIONAL RESULTS

In the absence of delay and with the flow rates and inlet concentrations chosen for the simulations, the calculations for the MBO system display hysteresis when the Br^- flow is used as an adjustable constraint. See Fig. 3 for a comparison of the calculated and experimental hysteresis.

With a delayed feedback present, the simulation displays a variety of complicated dynamics. In the presence of delay, the system exhibits (a) two coexisting stable stationary states (region A in Fig. 12), (b) a stable stationary state and a limit cycle (region B), (c) two coexisting limit cycles (region C), (d) a limit cycle and a chaotic attractor (region D), and (e) two distinct chaotic attractors (region E), and (f) chaotic attractors arising from a crisis (region F). As can be seen in the diagram, two independent types of attractors exist for most τ values: an attractor in a high range of *p*Br values and one in a low range of *p*Br values.

At low (< 25 s) delay times, both attractors originally exist as stable stationary states. As the delay is increased to ≈ 70 s, the low pBr attractor begins to bifurcate through a period doubling sequence. The lower attractor continues to bifurcate as the delay is increased further. The upper attractor rapidly goes through a period doubling sequence at a τ value of approximately 132 s. As the delay is increased, the upper attractor bifurcates further, until at a τ value near 180 s, the upper attractor undergoes a crisis as it merges with the lower attractor.

In Fig. 13, we show selected phase portraits for the transition through the crisis. Figure 13(a) at $\tau = 110$ s shows the upper attractor in a *P* 1 state and the lower attractor in a *Pn* state. At a τ value of 171.6 s [Fig. 13(b)], both the upper and lower attractors appear to be chaotic. With an increase of τ to 180.4 s, the upper attractor spirals past the fixed point and "merges" with the lower attractor [Fig. 13(c)]. This sequence is similar to what we see in experiments (Fig. 11). In the experiment, the onset of crisis occurred at or before $\tau = 109.85$ s.

ACKNOWLEDGMENT

This work was supported in part by the National Science Foundation and the National Institute of Health.

[1] D. J. Allwright, J. Math. Biol. **4**, 363 (1977); H. T. Banks and J. M. Mahaffy, Q. Appl. Math. **36**, 209 (1978); U. an der Heiden, J. Math. Anal. Appl. **70**, 599 (1979); J. M. Mahaffy, *ibid.* **72**, 24 (1980).
[2] L. Glass and M. C. Mackey, Ann. N. Y. Acad. Sci. **316**, 214 (1979); M. C. Mackey, Bull. Math. Biol. **41**, 829 (1979).
[3] M. C. Mackey and L. Glass, Science **197**, 287 (1977).
[4] F. Schürer, Math. Nachr. **1**, 295 (1948).
[5] K. Ikeda, Opt. Commun. **30**, 257 (1979); K. Ikeda, H. Daido, and O. Akimoto, Phys. Rev. Lett. **45**, 709 (1980); H. M. Gibbs, F. A. Hopf, D. L. Kaplan, and R. L. Shoemaker, *ibid.* **46**, 474 (1981); J. Y. Gao, L. M. Narducci, L. S. Schulman, M. Squicciarini, and J. M. Yuan, Phys. Rev. A **28**, 2910 (1983); P. Nardone, P. Mandel, and R. Kapral, *ibid.* **33**, 2465 (1986); R. Vallée and C. Delisle, *ibid.* **34**, 309 (1986).
[6] K. W. Smith and R. M. Noyes, J. Phys. Chem. **87**, 1520 (1983).
[7] M. Schell and J. Ross, J. Phys. Chem. **85**, 6489 (1986).
[8] I. R. Epstein, J. Phys. Chem. **92**, 1702 (1990).
[9] E. C. Zimmermann, M. Schell, and J. Ross, J. Chem. Phys. **81**, 1327 (1984).
[10] J. Weiner, F. W. Schneider, and K. Bar-Eli, J. Phys. Chem. **93**, 2704 (1989).
[11] J. Hale, *Theory of Functional Differential Equations* (Springer, New York, 1977); U. an der Heiden and M. C. Mackey, J. Math. Biol. **16**, 75 (1982); K. Ikeda and K. Matsumoto, J. Stat. Phys. **44**, 955 (1986); J. Hale and N. Sternberg, J. Comput. Phys. **77**, 221 (1988); N. MacDonald, *Biological Delay Systems: Linear Stability Theory* (Cambridge University, Cambridge, 1989).
[12] W. Geiseler and K. Bar-Eli, J. Phys. Chem. **85**, 908 (1981).
[13] W. Geiseler, Ber. Bunsenges. Phys. Chem. **86**, 721 (1982); J. Phys. Chem. **86**, 4394 (1982); K. Bar-Eli and W. J. Geiseler, *ibid.* **87**, 3769 (1983); C. E. Dateo, M. Orbán, P. De Kepper, and I. R. Epstein, J. Am. Chem. Soc. **104**, 504 (1982).
[14] P. Grassberger and I. Procaccia, Physica **9D**, 189 (1983); Phys. Rev. Lett. **50**, 349 (1983); Phys. Rev. A **28**, 2591 (1983); Physica **13D**, 34 (1984).
[15] M. Le Berre, E. Ressayre, A. Tallet, H. M. Gibbs, D. L. Kaplan, and M. H. Rose, Phys. Rev. A **35**, 4020 (1987).
[16] B. Dorizzi, B. Grammaticos, M. LeBerre, Y. Pomeau, E. Ressayre, and A. Tallet, Phys. Rev. A **35**, 328 (1987).
[17] As long as the delay does not change the location of the feedback curve, the steady states of the system with delay are the same as those of the system without delay. The delay *may* change the stability properties of the steady state. It can be shown [K. L. Cooke and Z. Grossman, J. Math. Anal. Appl. **86**, 592 (1982)] that the system may undergo arbitrarily many switches from stability to instability to stability as the delay increases.
[18] B. D. Hassard, N. D. Kazarinoff, and Y. H. Wan, *Theory and Applications of Hopf Bifurcation* (Cambridge University, Cambridge, 1981); J. Guckenheimer and P. Holmes, *Nonlinear Oscillations, Dynamical Systems, and Bifurcations of Vector Fields* (Springer, New York, 1983).
[19] J. Maurer and A. Libchaber, J. Phys. Lett. **40**, 419 (1979); J. P. Gollub and S. V. Benson, J. Fluid Mech. **100**, 449 (1980); M. Giglio, S. Musazzi, and V. Perini, Phys. Rev. Lett. **47**, 243 (1981).
[20] R. H. Simoyi, A. Wolf, and H. L. Swinney, Phys. Rev. Lett. **49**, 245 (1982).
[21] A. Longtin and J. G. Milton, Math. Biosci. **90**, 183 (1988).
[22] N. H. Packard, J. P. Crutchfield, J. D. Farmer, and R. S. Shaw, Phys. Rev. Lett. **45**, 712 (1980).
[23] F. Takens, in *Dynamical Systems of Turbulence*, edited by D. A. Rand and L. -S. Young (Springer, Berlin, 1981).
[24] C. W. Simm, M. L. Sawley, F. Skiff, and A. Pochelon, Helv. Phys. Acta **60**, 510 (1987).
[25] H. G. E. Hentschel and I. Procaccia, Physica **8D**, 435 (1983).
[26] P. Grassberger, Phys. Lett. A **97**, 227 (1983).
[27] See, e.g., *Dimensions and Entropies in Chaotic Systems*, edited by G. Mayer-Kress (Springer, Berlin, 1986).
[28] J. Theiler, Phys. Rev. A **34**, 2427 (1986).
[29] J. D. Farmer, Physica **4D**, 366 (1982).
[30] M. Le Berre, E. Ressayre, A. Tallet, and H. M. Gibbs, Phys. Rev. Lett. **56**, 274 (1986).
[31] J. Kaplan and J. Yorke, *Lecture Notes in Mathematics* (Springer-Verlag, Berlin, 1979), No. 730.
[32] A. M. Albano, J. Muench, C. Schwartz, A. I. Mees, and P. E. Rapp, Phys. Rev. A **38**, 3017 (1988).
[33] C. Grebogi, E. Ott, and J. A. Yorke, Phys. Rev. Lett. **48**, 1507 (1982).
[34] R. M. Noyes, R. J. Field, and R. C. Thompson, J. Am. Chem. Soc. **93**, 7315 (1971).
[35] J. J. Tyson, in *Oscillations and Travelling Waves in Chemical Systems*, edited by R. J. Field and M. Burger (Wiley-Interscience, New York, 1985).
[36] See, for example, B. Peng, S. K. Scott, and K. Showalter, J. Phys. Chem. **94**, 5243 (1990).
[37] S. K. Scott, B. Peng, A. S. Tomlin, and K. Showalter, J. Chem. Phys. **94**, 1134 (1991).